PPPL--2694

DE90 014810

Transport Simulations of TFTR Experiments to Test Theoretical Models for χ_e and χ_i

M. H. Redi and G. Bateman

Princeton Plasma Physics Laboratory

Princeton, NJ 08543

1-$\frac{1}{2}$-d BALDUR transport code predictions using recent theoretically-based models for thermal and particle transport are compared to measured profiles of electron plasma density and electron and ion temperatures for TFTR ohmic, L-mode and supershot discharges. The profile consistent drift wave model is found to overestimate ion temperatures at high heating powers, so that a third mode or loss process is needed in addition to drift wave

1. Introduction

Recent interest in understanding the basis of tokamak energy and particle transport has led to the development of theoretical models formulated specifically for testing in predictive tokamak transport codes. With a predictive transport code, measured plasma temperatures and density can be compared to those predicted from a self-consistent, time-dependent calculation of plasma heating, fuelling, conduction, radiation, *etc.* The same code can then be used for predicting performance of future machines (*e.g.*, CIT, ITER, ARIES) and to test ways of improving transport in actual experiments. It is not practical to do extensive testing of transport models against a global database of plasma profiles with a large predictive code such as BALDUR, but by examining only cases typical of three TFTR regimes (ohmic, L-mode, and supershot), insight into the main features of particular models can be gained. In this article, temperatures are predicted and compared to data rather than fluxes or transport coefficients because we take the point of view that the experimental measurements are the fundamental reference point in validating theory. Temperatures are measured not fluxes or diffusivities.

Attempts to model experiments with predictive transport codes and theoretically-

based models have led to the development of increasingly complex models. Yet the elements of a) drift wave transport (due both to trapped electron and η_i modes) as well as b) a semiempirical edge loss model are common to most of the recent work in this area [1–11]. Dominguez and Waltz[3] devised the semi-empirical tearing-mode-based "venetian blind model" to model edge losses in ohmic and neutral beam heated plasmas on Doublet III. Confinement of plasmas on ISX-A, Alcator-A, Alcator-C, and JET was also simulated with this model. Romanelli *et al.* [5] used a q-dependent semiempirical form factor for plasma edge losses in ohmic plasmas on Doublet III and to estimate confinement scaling for PDX, Doublet III, Alcator-A, and Alcator-C.

We test several models based on this common hypothesis that two modes are primarily responsible for overall transport. We find that none of the transport models can simulate all three types of TFTR experiments with good agreement. We suggest one possible new mechanism to incorporate in future simulations with each model.

Two recent theoretically-based models which have been notably successful in predicting tokamak behavior are the profile consistent drift wave model

(PCDW) [1] and the multiple mode model (MMM)[11]. In PCDW edge transport is provided through the consequences of assuming profile consistency. PCDW shows good agreement with experimental temperature profiles found for ohmic, saturated ohmic, ohmic pellet, L-mode, and low power supershots from TFTR; ohmic and ohmic pellet cases from ASDEX, Alcator-C, TEXT [2,7–10]. MMM relies on an early (1978) model of resistive ballooning for edge transport losses[12]. We construct another multimode type model (MMCD) with a recent model of resistive ballooning losses (Carreras, Diamond[13]) which incorporates the effects of different scales for velocity and magnetic field fluctuations. The primary goal of this paper is a comparison of the predictions of these theoretically based models against measured electron and ion temperatures from TFTR experiments.

The models tested are dependent on the source terms calculated in the widely used 1-1/2-d BALDUR code, based on an extensively documented and tested 1-d version. The three experiments simulated were chosen to be representative of typical TFTR experiments for which a complete set of measurements, particularly electron and ion temperatures were available.

The paper is organized as follows. In Sec. 2, the models are described in

detail. In Sec. 3, the experiments are discussed. Details of the simulation procedure with the transport code are presented in Sec. 4. Results are discussed in Sec. 5 and the conclusions and summary are found in Sec. 6.

2. Theoretical Models

Three models for tokamak transport are described below; the profile consistent drift wave model in Sec. 2.1 and two versions of multiple mode models in Sec. 2.2.

2.1. The Profile Consistent Drift Wave Model

The profile consistent drift wave model (PCDW) was developed by W.M. Tang [1]. This model uses global drift wave scaling and an empirical form factor to produce the observed radial form of the thermal diffusivities. The model was first tested against TFTR ohmic data and was modified to include the effects of significant radiative losses [2]. Overall numerical factors for electron and ion losses were calibrated against this data in the neo-Alcator regime (dominated by electron losses) and in the saturated ohmic regime (both electron and ion losses significant).

PCDW was then successfully applied to simulation of pellet-fuelled ohmic plasmas on TEXT [7], Alcator-C and ASDEX [8]. Suppression of η_i- mode ion transport in the dissipative trapped electron mode regime (DTEM) was seen in these cases. The model was then used for predictions of neutral beam heated plasmas [9]. T_{eo} and τ_E were found to be in good agreement even for the first TFTR supershot where the simulation indicated ν_e^* was low (CTEM) and $\eta_i < \eta_i^c$. Here $\eta_i = \frac{d\ell n T_i}{d\ell n n_i}$, and η_i^c is a critical threshold, typically = 1.5. When ion temperature profiles became available on TFTR in 1988, it was found that the model predicted overly broad profiles for ion temperatures. Kinetic microinstability studies had shown that $\chi_i \sim \chi_e$ for CTEM [1,14]. This was subsequently incorporated into the model by dividing the transport losses of the previous $\chi_e^{\rm CTEM}$ between χ_e^{CTEM} and χ_i^{CTEM}, so that both electron and ion losses are included in the CTEM regime. With this new CTEM feature, simulations with the PCDW model were found to give good agreement with T-10 high power ECH data [9], as well as for six TFTR supershot discharges [10].

With these developments, the PCDW model for anomalous electron and ion transport can be summarized as follows: The anomalous electron trans-

port arises entirely from the trapped electron mode,

$$\chi_e^{\rm ANOM} = \chi_e^{\rm TEM}$$

with

$$\chi_e^{\rm TEM} = \begin{cases} \frac{0.47(1+0.25\alpha_n)P_{tot,e}^{0.8}F_{H,e}(r)}{n_{eo}R_o^{1.2}a^{0.1}B_o^{0.4}q(a)^{0.9}Z_{eff}^{0.2}} & \text{if } \nu_e^* \geq 0.15, \\ \frac{0.33(P_{tot,e}/n_{eo})^{0.6}F_{H,e}(r)}{a^{0.2}(R_oB_oq(a))^{0.8}} & \text{if } \nu_e^* < 0.15. \end{cases}$$

The anomalous ion transport arises from both the η_i-mode and the trapped electron mode,

$$\chi_i^{\rm ANOM} = \chi_i^{\eta_i} + \chi_i^{\rm TEM}$$

where,

$$\chi_i^{\eta_i} = \begin{cases} \frac{0.5(P_{tot,i}/n_{io})^{0.6}F_{H,i}(r)}{a^{0.2}(R_oB_oq(a))^{0.8}} & \text{if } \langle\eta_i\rangle \geq 1.5, \\ 0 & \text{if } \langle\eta_i\rangle < 1.5 \end{cases}$$

and

$$\chi_i^{TEM} = \begin{cases} 0 & \text{if } \nu_e^* \geq 0.15, \\ 1.5\left[\frac{(|L_n|+|L_{T_i}|)}{R_o}\right]_{q=1.5}\chi_e^{\rm TEM} & \text{if } \nu_e^* < 0.15. \end{cases}$$

with

$$F_{Hj}(r) = \frac{(1-e^{-\alpha_q})\exp(2\alpha_q r^2/3a^2)\int_o^r h_j(r)r\,dr}{(n_j/n_{jo})(r^2/a^2)\int_0^a h_j(r)r\,dr},$$

and $\alpha_q = q(a) + 0.5$. $h_j(r)$ is the net local heating power density for species j from OH, NBI, ICRH, Q_{ie}, *etc.*, minus the radiated power (for electrons).

$$P_{tot,j} = (2\pi)^2 R_o \int_0^a h_j(r) r \, dr$$

is the integrated heating power, in MW, for species j.

$$\alpha_n = \frac{(n_{eo} - n_e(a))}{(\langle n_e \rangle - n_e(a))} - 1$$

is a measure of the density peakedness, where

$$\langle n_e \rangle = (2/a^2) \int_0^a n_e(r) r \, dr.$$

ν_e^* is evaluated at q = 1.5 and

$$\langle \eta_i \rangle = \frac{T_i(q=1) - T_i(q=2)}{T_i(q=1.5)} \; \frac{n_i(q=1.5)}{n_i(q=1) - n_i(q=2)},$$

is an average η_i between the q = 1 and 2 surfaces. All χ are in m^2/s, R_o and a in m, B_o in T, and densities in $10^{20} m^{-3}$. L_T is the scale length for the plasma ion temperature $= -[\frac{d\ell n T_i}{dr}]^{-1}$, and L_n is the scale length for the plasma density. When ν_{*e} at the q = 1.5 surface is greater or less than 0.15, the dissipative trapped electron mode (DTEM) or collisionless trapped electron mode (CTEM) losses are expected to dominate and control the magnitude and scaling of the TEM plasma transport coefficients. When η_i is greater

than some critical value, taken to be 1.5 in all simulations for PCDW, the ion diffusivity is increased by $\chi_i^{\eta_i}$ to describe η_i mode losses. No PCDW particle transport coefficient has been derived. Empirical D, v were used to match experimentally observed density profiles.

The model was derived under the assumption that temperature profiles are approximately Gaussian and depend on plasma current through $T_e(r) \sim \exp[-(q(a) + 0.5)\ r^2/a^2]$. This empirically based, "profile consistency" assumption leads to the result that drift wave transport determines plasma confinement depending on the values of the electron collisionality and η_i in the confinement regime, q = 1 to 2. The local plasma temperature is assumed to depend on the global variable q(a) and the PCDW diffusivities are effectively nonlocal.

Table 1 summarizes the work done to this point with PCDW. All experiments have been simulated with the model described above, called the "species specific heating model" in Refs. [2,8]. Small changes have been made in the numerical prefactors used for PCDW. It was found that the central plasma resistance in the earlier simulations had been artificially increased to round the current profile. This decreased the central electron temper-

ature by 5%. The CTEM coefficient was halved, motivated by the above discussion; see also Refs. [1,10,14]. The coefficients are then $[C_F, C_G, C_H] = [0.78, 0.33, 0.5]$. A large number and variety of discharges on TFTR and other tokamaks have been successfully simulated with this model using the BALDUR code.

2.2. *Multiple Mode Models MMM and MMCD*

Development of a theoretically-based purely local transport model was facilitated by the appearance of the Ross report [15] in 1987, a compendium of local transport coefficients based on a wide variety of possible instabilities. Motivated by the work of J. Sheffield [6], C. E. Singer proposed the multiple mode model, a linear sum over transport from several local modes [11]. In this paper are presented the results of simulations with his benchmark version [4], called here MMM and for the benchmark version using the new Carreras-Diamond [13] model for resistive ballooning transport, called here MMCD.

The multiple mode models incorporate many of the ideas found useful in PCDW, without the assumption of profile consistency: (1) Confinement for all cases is controlled by driftwave and η_i losses; (2) at low electron collision-

ality, turning η_i losses off gives good agreement for supershot temperatures; (3) the combination of η_i losses and collisional drift wave losses gives rise to anomic and L-mode transport. In these models (both MMM and MMCD), the heat fluxes are predicted to arise from a combination of driftwave, rippling mode and resistive ballooning modes

$$Q_e^{ANOM} = Q_e^{dw} + Q_e^{rm} + Q_e^{rb}$$
$$Q_i^{ANOM} = Q_i^{dw} + Q_i^{rm} + Q_i^{rb}.$$

For drift waves

$$Q_e^{dw} = f_e^{dw}(5/2 - 3/2\, f_{ith})\hat{D}_{te}\, f_\beta\, n_e\, \partial T_e/\partial r$$
$$Q_i^{dw} = f_i^{dw}\, 5/2(\hat{D}_{te} + f_{ith}\hat{D}_i)\, f_\beta\, n_i\, \partial T_i/\partial r.$$

In MMM,

$$\hat{D}_{te} = (r/R)^{1/2}\omega_e^*/k^2{}_\perp \min[1, \omega_e^*/\nu_{eff}].$$

The transition between the collisionless and collisional trapped electron modes follows the Dominguez-Waltz model [3], although recent work [16] suggests a more detailed treatment of the local collisionality may be necessary. A different trapped electron collisionality condition is used in MMCD [17,18]

$$\hat{D}_{te} = \epsilon^{1/2}\, \frac{\omega_e^*}{k_\perp^2}\left[1.0, \frac{0.1}{\nu_e^*}\right]_{min}.$$

For both MMM and MMCD, the η_i mode gives rise to the coefficient

$$\hat{D}_i = \omega_e^*/k_\perp^2[(2T_i/T_e)(L_n/L_{Ti})(L_n/R)]^{1/2}.$$

The η_i threshold function is

$$f_{ith} = [1 + \exp^{-6(\eta_i - \eta_i^{th})}]^{-1}.$$

The Romanelli η_i threshold has been used

$$\eta_i^{th} = \max\left[\eta_{ic} + 2.5\left(\frac{Ln}{R_o} - 0.2\right)\right]$$

and $\eta_{ic} = 1.0$ except where noted. A finite β' correction [15,16]

$$f_\beta = (1 + \beta'/\beta'_{cl})/[1 + (\beta'/\beta'_{cl})^3]$$

is also included.

The anomalous electron ion energy exchange

$$\Delta^{DR} = 0.3\left(0.89 - 0.54\eta_i - 0.6\frac{\beta'}{\beta'_{ci}}\right)D^{DR}\,\frac{n_e T_e}{L_n^2}$$

where

$$D^{DR} = f_\beta\left(1 - \frac{f_{ith}}{0.95 + \nu_e^*}\right)\hat{D}_{te}$$

has been included in all simulations with multiple mode models. MMM and MMCD include the convective energy losses associated with particle transport as well as conductive losses in $\chi_{e,i}^{eff}$. The $\chi_{e,i}^{eff}$ will be written as $\chi_{e,i}$.

The rippling mode losses are described in Refs. [4,11], but the rippling mode contribution to transport in this study is so small that the details of the model will not be given here.

The resistive ballooning mode in the original model (MMM) [4,11] was given by

$$Q_e^{rb} = f_e^{rb} \Lambda_s^2 \chi_e^{rb} n_e \partial T_e / \partial r$$

where

$$\chi_e^{rb} = \frac{3 v_{the} \eta_{spitzer} (\beta_q^2 L_s / L_p)^{3/2}}{2\mu_o (2q)^{1/2} v_{alfven}}$$

and

$$\Lambda_s = 4/3\pi \ell n \left[R v_{alfven} \mu_o / \eta_{spitzer} \beta^{1/2} \right].$$

The scale heights are

$$L_s = R q / [r/q \, \partial q / \partial r]$$

and

$$L_p = (r/p \, \partial p / \partial r)^{-1}.$$

The enhancement factor Λ_s was added by Singer to the Carreras *et al.* model. This factor takes into account the different characteristic scale sizes of magnetic and velocity fluctuations in tokamak plasmas. We found Λ_s about 10

in simulations of the three TFTR cases studied here, with Λ_s^2 enhancing edge transport by two orders of magnitude.

MMCD uses a more recent model of resistive ballooning mode transport [12,19,20] given by

$$\chi_e^{RB} = f_e^{rb} \frac{1}{2^{13/6}\langle\eta\rangle^{2/3} S^{2/3} \hat{S}} \left(\beta \frac{R_o^2}{L_p R_c} q^2\right)^{4/3} \frac{v_e r^2}{R_o} \Lambda^{4/3} f_{dia} + \frac{\beta R_o^2 q^2}{\sqrt{2} L_p R_c S} \frac{r^2}{\tau_R} \Lambda^2 f_{dia},$$

$$D^{RB} = f_a^{rb} \frac{\beta R_o^2 q^2}{\sqrt{2} L_p R_c S} \frac{r^2}{\tau_R} \Lambda^2 f_{dia}.$$

The ion thermal diffusivity has been chosen to be proportional to the particle diffisivity

$$\chi_i^{RB} = f_i^{rb} \frac{\beta R_o^2 q^2}{\sqrt{2} L_p R_c S} \frac{r^2}{\tau_R} \Lambda^2 f^{dia}.$$

Here, the diamagnetic stabilization term is approximated by

$$f_{dia} = \left[1 + \left(\frac{\mu_o \omega_{ci} \rho_i^3}{\eta \beta q^2 L_{ni}}\right)^2\right]^{-1/6}.$$

$\hat{S}$ is the plasma shear. The magnetic Reynold's number is defined by S $= \tau_R/\tau_{hp}$, $\tau_R = r^2\mu_0/\eta \equiv$ local resistive time, with $\eta =$ the local Spitzer resistivity and $\tau_{hp} = R_o/v_A \equiv$ local poloidal Alfven time.

R_c is the radius of curvature, taken to be the major radius. The multiplier

Λ is the solution to the equation

$$\Lambda = \frac{2}{3\pi} \ln\left[\frac{256 S^2 L_p}{\beta R_o \Lambda^3} \left(\frac{\hat{S}}{\langle n \rangle}\right)^4\right].$$

We use average toroidal mode number $< n >$ equal to 2. The enhancement factor, Λ, is now found to be 4 to 7 in the TFTR cases studied. The new version of resistive ballooning transport is enhanced by $\Lambda^{4/3}$ rather than Λ_S^2. MMCD also includes pressure driven $\tilde{E} \times \tilde{B}$ flux in χ_e^{rb}, χ_i^{rb} and D^{rb} enhanced by Λ^2 [19].

The pre-multiplying numerical factors used here for MMM and MMCD, are the ones obtained by Singer *et al.*[4] in fitting ASDEX L-mode and L-mode data base confinement scalings: $[f_{i,e}^{dw}, f_{i,e}^{rm}, f_{i,e}^{rb}] = [0.3, 3.0, 1.0]$ except where noted in Sec. 5.3.

3. TFTR Experiments Simulated

Three representative TFTR experiments have been simulated with the PCDW, MMM and MMCD models. Simulation results are presented in Sec. 5 for TFTR ohmic shot 31819, L-mode shot 41326, and supershot 30640. 31819 is a medium density ohmic discharge, 41326 is a high power L-mode without significant MHD or carbon blooms and 30640 is an early (1988)

moderate power supershot. In Table 2 are shown the plasma parameters for these experiments.

4. The Transport Code Simulations

The 1-1/2 dimensional BALDUR transport code was used for all simulations with the PCDW, MMM and MMCD models. Several similar supershot and ohmic cases had been studied previously with the 1-d version of BALDUR [21,22] to evaluate the performance of the profile consistent model in predicting TFTR data. When simulating the ohmic TFTR experiments with PCDW, the 1-1/2-d code was found to give results essentially unchanged from the 1-d version. Because of differences in 1-1/2-d BALDUR compared to 1-d BALDUR, the 1-1/2-d calculations of T_e and T_i for the TFTR supershot are 10% below the values obtained with 1-d BALDUR [9,10]. The multiple mode model (MMM) transport calculations were obtained from a subroutine for BALDUR written by Singer and Ghanem.

For ohmic simulations, a concentric circular flux surface equilibrium was assumed, while for the supershot cases the effects of Shafranov shift were handled by the Lao VMOMS harmonic equilibrium code [23]. Line average

electron density was maintained in the ohmic cases by gas puff and density monitor. Simulations included neoclassical particle and thermal transport ($\chi_i^{\text{Chang-Hinton}}$ for ions) in addition to anomalous transport.

Sawteeth were included *via* a Kadomtsev sawtooth model with sawtooth period matched to experiment for the ohmic and L-mode phases. In the next section, simulated temperatures are compared to Thompson electron temperature profile measurements and to charge exchange recombination spectroscopy (CHERS) ion temperature profile measurements. The relative sawtooth phase can be important in comparing simulation to measurement. In ohmic case 31819, a small plasma, T_{eo} varies by only 3% during a sawtooth period. For L-mode shot 41326, the sawtooth period is much larger (200 msec. *vs.* 25 msec.), and the sawtooth excursion causes 10% changes in n_{eo} and T_{eo}. The L-mode simulations were sawtooth phased to the experiment. Sawteeth are not present in the supershot experiment.

5. Simulation Results

5.1. Particle Transport Results

For PCDW simulations an empirical particle transport model was used to reach within 10% of the measured central and line average electron densities. These density profiles are shown as solid curves in Figs.1-3. A supershot density profile (Fig. 3) was obtained with the PCDW empirical particle transport model: $D \propto 1/n_e(r)$, and $V_{impurity} \propto D \times r/a^2$. The edge densities and temperatures were taken to agree with poloidally averaged edge values. The recycling coefficients were set equal to 0.9 for all phases except supershot where R = 0.8, consistent with analysis using the DEGAS neutral transport code [24]. The particle transport model used for PCDW, MMM, and MMCD use the same edge densities, temperatures and recycling. In Figs. 1-3 are also shown comparisons of measured electron densities to those predicted by MMM and MMCD for ohmic, L-mode, and supershot simulations.

MMM predicts L-mode particle transport quite well but does not give such good agreement for electron density predictions of ohmic and supershots (dotted curves, Figs. 1-3). MMM was designed to simulate the ASDEX L-

mode and was expected to give good agreement for TFTR L-mode cases.

MMCD improves the MMM predictions of particle transport for the ohmic and supershot cases, without destroying the model's good simulation of particle transport for L-mode (dashed curves, Figs. 1-3). Although the predictions of the supershot density profile were not as good as with the empirical model, the MMM and MMCD particle transport models were retained in order to present a consistent set of simulations.

5.2. *Profile Consistent Drift Wave Model Results*

Figure 4 shows a comparison of electron and ion temperatures to PCDW simulation predictions for the three TFTR cases (solid curves). The predicted electron temperatures are within 10-20% of the measured values. Detailed results for simulations of TFTR ohmic electron temperatures with the profile consistent model have already been published [4,6]. PCDW was calibrated on TFTR ohmic plasmas to give agreement with magnetic confinement time data and electron temperature profiles. Thus, it was expected that simulation of ohmic shot 31819, for which ion temperature profile data was available, would give good agreement for both electron and ion temperature predictions

(Figs. 4(a),(b)).

In Fig. 4, we see the low power supershot 30640 ion temperature is well represented by the PCDW simulation, but the high power L-mode ion temperature measurements are much lower than predicted. PCDW works well for simulating TFTR experiments at low heating power (< 14 MW) (see also [6,8]). Recent work by Taroni [25] indicates that PCDW underestimates transport losses for JET experiments with high heating power. Mikkelsen [26] at TFTR also finds better agreement at low heating powers (5 MW).

The PCDW collisionality for the supershot case (Table 3) is $\nu_{*e} < 0.15$ as found in the experiment. The L-mode simulation, however, overestimates the plasma temperatures, and we find $\nu_{*e} = 0.09$ where CTEM should apply. If χ_i^{ANOM} is increased to predict the measured T_{io}, $\nu_{*e} > 0.15$ as for DTEM. PCDW lacks a mechanism for increased ion transport losses in DTEM at high heating power.

In Table 3 are shown the simulated conductive, convective, radiative, and neutral losses as well as ohmic and neutral beam heating and the classical electron-ion interchange losses for the three TFTR experiments at $r = a/2$. PCDW simulations used the convective mulitplier $= 3/2$. Electron losses ex-

ceed ion losses for the ohmic plasma. With PCDW the ion conduction losses are somewhat smaller than electron conduction losses in L-mode and in the supershot (Table 3). We note from the PCDW results that convective losses in the supershot simulation are much greater than for L-mode and ohmic. Figure 5(a) shows the evolution of the central electron and ion temperatures for the PCDW supershot case. Low collisionality and low η_i (Table 3) cause the final temperatures to be in agreement with experiment (Table 4) within 15%.

Figure 6 shows the anomalous χ_e and χ_i for simulations with this model and that $\chi_e > \chi_i$ for ohmic and L-mode but $\chi_e \approx \chi_i$ for the supershot. Goldston [27] showed in initial studies of TFTR ohmic discharges that $\chi_e > \chi_i$. Increased χ_i would improve agreement for the PCDW results on the L-mode case. Zarnstorff *et al.* [28] have shown that $\chi_i > \chi_e$ for TFTR L-mode; Zarnstorff has also shown that $\chi_i \sim \chi_e$ for TFTR supershots [28].

In Table 4, we compare some scalar experimental quantities to PCDW simulation results. PCDW fails to successfully predict the plasma temperatures of high power L-mode shot 41326 and overestimates τ_E^{th}. We might ask if the data for this shot exhibit any new types of transport losses not included

in PCDW. In fact, TFTR performance at high beta is now primarily limited by MHD or carbon influx (carbon bloom) in which resultant radiation limits high power performance [29,30]. Recently, Redi and Cohen [31] have proposed a model of MHD-enhanced transport near the beta limit. However, shot 41326 has a typical L-mode confinement, and has neither strong MHD behavior [32] nor a carbon bloom. Anomalous losses of fast ions at high beam power remains one possible cause of the degradation of confinement from that predicted by PCDW, but the underlying basis for such losses is not clear.

5.3. *Multiple Mode Model Results*

The emphasis will be on MMCD predictions for thermal transport in this section as the development of MMCD supercedes MMM. Simulations parallel to those of Sec. 5.2 with PCDW were carried out with both MMM and MMCD for the three TFTR experiments. In Table 4, the central plasma temperatures are compared to experiment for all three models. Predicted electron and ion temperatures are compared to data in Fig. 4 for MMCD (dashed curves). The ohmic electron temperature profile is very well simu-

lated by MMCD (Fig. 4(a)). The ohmic central ion temperature is underestimated (Fig. 4(b)). The L-mode electron and ion temperatures are broader than measured (Fig. 4(c),(d)). The model, which does match central temperatures, significantly overestimates τ_E^{th} in ohmic and L-mode cases because the ion temperature profiles are too broad (Table 4).

Simulation of the TFTR supershot with MMCD (Fig. 4(e),(f)) is found to overestimate both electron and ion thermal transport by about a factor at least 3 (see below). The anomalous χ_e and χ_i are shown in Fig. 7 for MMCD simulations of the three TFTR experiments. Note that χ_i and χ_e are very large in the supershot case (Figs. 7(e),(f) dashed curves) because convective as well as conductive losses are included in effective diffusivities for this model.

The drift wave (TEM=triangles, η_i=crosses) and resistive ballooning (squares) contributions are shown in Fig. 7 for each case. Central transport is dominated by drift wave losses with significant edge electron losses arising from the resistive ballooning mode. The η_i contribution to χ_e in each case drops below zero, illustrating the development of an inward pinch from the η_i mode. Resistive ballooning modes destroy magnetic surfaces and so allow fast elec-

tron transport out of the plasma. Slower ion motion leads to smaller ion losses. The resistive ballooning mode does not lead to significant ion energy losses at the plasma edge. The plasma ion temperature predicted is much broader than the electron temperature. Although the electron temperature profiles for L-mode and supershot could be narrowed by increasing the resistive ballooning transport, the ion temperatures would not be narrowed. The rippling mode contributions are so small as not to appear in the figures.

For MMM and MMCD, the evolution of the central electron temperatures for shot 30640 from ohmic to supershot phase are shown in Fig. 6 (b,c). All models predict the ohmic phase central temperature in agreement with the ECE measured peak ohmic electron temperature, 6.3 ± 0.3keV. The MMM final T_{io} is 18 keV, in better agreement with experiment than MMCD! In comparison with MMM, MMCD includes a smooth transition to CTEM *via* ν_e^*, but T_{io} is still much lower than measured. This simulation results in T_{eo} = 4.5 keV and T_{io} = 10 keV.

Several years ago, Cheng and Tsang [33], and Gribkov *et al.* [34] showed that the η_i mode threshold increases rapidly with T_i/T_e. This ratio is about 4 in the supershot. To explore this, we increase the η_i^c threshold to 10 and find

that a high supershot temperature can be predicted by MMCD, if trapped electron thermal (not particle) drift wave losses are reduced by 1/3 (T_{eo} = 6.4 keV, T_{io} = 27 keV). These predictions are shown as long dashed curves in Figure 4 (MMCD'). This model also gives reasonable results in the ohmic phase with $\eta_i^c = 1.0$, (T_{eo} = 3.6 keV and T_{io} = 2.2 keV) but causes the model to significantly overestimate the plasma temperatures in L-mode (T_{eo} = 5.3 keV and T_{io} = 9.1 keV).

Modifying the η_i model and increasing the η_i losses will not reduce the L-mode electron temperature. No adjustment of the drift wave transport coefficients can be found to fit both L-mode and supershot plasma temperatures because the trapped electron collisionality condition $\nu_e^* < 0.1$ is only satisfied in shot 30640 for 12cm < r < 50 cm. Thus, DTEM governs the central supershot electron temperature and the PCDW improved behavior of CTEM ($T^{\frac{5}{2}}$) vs. DTEM ($T^{\frac{7}{2}}$) transport cannot be obtained with this model unless DTEM transport is reduced or the collisionality condition is modified. Preliminary multimode simulations of the TFTR supershot with a toroidal CTEM model stabilized by L_n [35] give good agreement with the measured central electron temperature [36].

6. Conclusions

Considerable progress has been made in the last few years in understanding tokamak transport. We have shown that theoretically based models with empirical elements can be used to simulate TFTR experiments with some success, yet many discrepancies remain. In fact, the theories on which these models are based may not even apply to the highly nonlinear, fully developed strong turbulent conditions thought to occur in the plasma core. In particular, quasilinear models for weak turbulence effects are valid only for modes with $\gamma < \omega_*$ such as TEM.

The profile consistent drift wave model, with edge transport arising from the consequences of assuming profile consistency, has been found valid for simulating a large number of TFTR experiments. For high power cases, ion temperatures are overestimated with PCDW so that a "third mode" for anomalous losses of fast ions is proposed. In addition, a PCDW particle transport model is needed as is justification for the profile consistency assumption.

It had been hoped that since MMCD incorporates several of the key points of PCDW, it should be able to duplicate the successes of that model. By im-

proving the criteria for the DTEM/CTEM transition and for suppression of η_i mode losses, it seemed likely that this type of model could be successful in simulating low power supershot electron temperatures as well as L-mode and ohmic. In this paper, however, we have shown that PCDW fails to predict the high power L-mode temperatures and also that good multimode predictions of both L-mode and supershot plasma temperatures are not possible with the current DTEM/CTEM model. TEM transport in the supershot must be reduced compared to L-mode, perhaps by L_n stabilization. Thus, new transport mechanisms are required to understand high heating power discharges with either type of model. In addition, the broad ion temperature profiles predicted by MMCD, show that a new ion edge loss mechanism must be found if we are to model plasma transport by a linear combination of locally acting plasma modes.

In conclusion, none of the models tested were found to predict plasma temperatures within 20% for all three typical TFTR ohmic, L-mode, and supershot discharges. Present models for drift wave transport plus edge losses are not sufficient to predict tokamak confinement on TFTR.

Acknowledgments

It is a pleasure to acknowledge useful discussions of the theoretical models with C.E. Singer, W.M. Tang, B. Carreras, P.H. Diamond and R. Dominguez. Thanks are also due to C. Barnes, M. Bell, R. Budny, R. Fonck, E. Fredrickson, G. Hammett, D. Johnson, K. McGuire, D.R. Mikkelsen, H. Park, E. Synakowski, G. Taylor, F. Waelbroeck and M.C. Zarnstorff for discussions and use of TFTR data and to R.J. Goldston for suggesting the project.

This work was supported by the U.S. Department of Energy Contract No. DE-AC02-76-CHO3073.

References

[1] W.M. Tang, "Microinstability-based model for Anomalous Thermal Confinement in Tokamaks," Nucl. Fusion **26** (12) (1986) 1605-1618. B1 (1989) 1011-1017.

[2] M.H. Redi, W.M. Tang, P.C. Efthimion, D.R. Mikkelson, G.L. Schmidt, "Transport Simulations of Ohmic TFTR Experiments with Microinstability based Profile Consistent Models for Electron and Ion Transport," Nucl. Fusion **27** (12) (1987) 2001-2017.

[3] R. Dominguez and R.E. Waltz, "Tokamak Transport Code Simulation with Drift Wave Models," Nucl. Fusion **27** (1987) 65-79.

[4] C.E. Singer, E.S. Ghanem, G. Bateman, and D.P. Stotler, "Multiple Mode Model of Tokamak Transport," Princeton Plasma Physics Laboratory Report No. PPPL-2631 (1989) 12 pp.; Nucl. Fusion (in press).

[5] F. Romanelli, W.M. Tang, R.B. White "Anomalous Thermal Confinement in Ohmically Heated Tokamaks" Princeton Plasma Physics Laboratory Report No. 2310 (1986); Nucl. Fusion (1987).

[6] J. Sheffield, "Tokamak Transport in the Presence of Multiple Mechanisms," Nucl. Fusion (1989).

[7] D.L. Brower, M.H. Redi, W.M. Tang, R.V. Bravenec, R.D. Durst, *et al.*, "Experimental Evidence for Ion Pressure Gradient Driven Turbulence in TEXT," Nucl. Fusion **29** (1989) 1247-1254.

[8] M.H. Redi, W.M. Tang, D.K. Owens, M. Greenwald, O. Gruber, M. Kaufmann, "Transport Simulations of Ohmic Pellet Experiments on the TFTR, ASDEX, and ALCATOR-C Tokamaks," Princeton Plasma Physics Laboratory Report No. PPPL-2525 (July 1988) 42 pp., Fus. Tech. in press.

[9] W.M. Tang, C.M. Bishop, B. Coppi, S.M. Kaye, F.M. Perkins, *et al.*, "Microinstability-based Models for Confinement Properties and Ignition Criterion in Tokamaks," Princeton Plasma Physics Laboratory Report No. PPPL-2418, Proceedings of the Eleventh International Conference on Plasma Physics and Controlled Nuclear Fusion Research, (Kyoto, Japan, November 1986) (IAEA, Vienna, Austria), Vol 1, 337-344 (1987).

[10] W.M. Tang, N. Bretz, T.S. Hahm, W.W.Lee, F.W. Perkins, *et al.*, "The-

oretical Studies of Enhanced Confinement Properties in Tokamaks," Princeton Plasma Physics Laboratory Report No. PPPL-2580; IAEA, Nice, 1988.

[11] C.E. Singer, "Theoretical Particle and Energy Flux Formulas for Tokamaks," Comments Plasma Physics Controlled Fusion **11** (1988) 165-182.

[12] B.A. Carreras, P.H. Diamond, M. Murakami, J.L. Dunlap, J.D. Bell, *et al.*, "Transport Effects Induced by Resistive Ballooning Modes and Comparison with High-βp ISX-B Tokamak Confinement," Phys. Rev. Lett. **50** (1983) 503-506.

[13] B.A. Carreras, P.H. Diamond, "Thermal Diffusivity Induced by Resistive Pressure-Gradient-Driven Turbulence," *Phys. Fluids (1989).*

[14] G. Rewoldt, W.M. Tang, "Toroidal Microinstability Studies of High Temperature Tokamaks," Princeton Plasma Physics Laboratory Report No. PPPL-2635 (1989), Phys. Fluids **B2** (1990) 318-323.

[15] D.W. Ross, P.H. Diamond, J.F. Drake, F.L. Hinton, F.W. Perkins, et al., "Thermal and Particle Transport in Tokamaks – Theoretical models for Ignition Studies," FRCR No. 295, U. of Texas (1987) 33 pp.

[16] R.W. Waltz and R.R. Dominguez, "Note on Detailed Models for Trapped Electron Transport in Tokamaks,' Phys. Fluids B1 (1989) 1935-1937.

[17] G. Rewoldt, "Alpha particle effects on high-n instabilities in tokamaks," Phys. Fluids **31** (1988) 3727-3737.

[18] G. Rewoldt, W. M. Tang, R.J.Hastie,"Collisional Effects on Kinetic Electromagnetic Modes and Associated Quasilinear Transport", Phys. Fluids **30**,807 (1987).

[19] B.A. Carreras, private communication (1990).

[20] P.H. Diamond, private communication (1990).

[21] C.E. Singer, D.E. Post, D.R. Mikkelsen, M.H. Redi, A. McKenney, "BALDUR: A One-Dimensional Plasma Transport Code," Computer Phys. Comm. **49** (1988)275-398.

[22] M.H. Redi, "Standard Test Cases for the BALDUR Transport Code," Computer Phys. Comm. **49** (1988) 399-407.

[23] L. L. Lao, S. P. Hirschman, R. M. Wieland, Phys. Fluids **24** (1981) 1431.

[24] R.V. Budny, private communication (1990).

[25] T. Taroni, IAEA Workshop on Plasma Transport Measurement and Analysis:IAEA - W16, Princeton, N.J., November, 1989.

[26] D.R. Mikkelsen,"Comparison of Predicted and Measured Temperature Profiles in TFTR Plasmas", Bull. Am. Phys. Soc. **34**, (1989) paper 4Q08; Transport Task Force Meeting, Hilton Head, SC (1990).

[27] R.J. Goldston,Y. Tokase, M. Bell, M. Bitter, A. Cavallo, *et al.*, Proceedings of the 15th European Conference on Controlled Fusion and Plasma Heating, Dubrovnik (1988) Part I, p.99-102.

[28] M.C. Zarnstorff, V. Arunasalam, C.W. Barnes, M.G. Bell, M. Bitter, *et al.*, Proceedings of the Twelfth International Conference on Plasma Physics and Controlled Nuclear Fusion Research, (Nice, France, October 1988) (IAEA, Vienna, Austria), Paper IAEA-CN-50/A-III-3.

[29] D.W. Johnson, S.D.Scott, C.W. Barnes, M. Bell, M. Bitter,*et. al.* Proceedings of the 17th European Conference on Controlled Fusion and Plasma Heating, Amsterdam, the Netherlands (1990).

[30] M. Ulrickson, Proceedings of the 9th PSI Conference. Bournemouth. UK (1990).

[31] M.H. Redi, S.A. Cohen, Princeton Plasma Physics Laboratory Report No. PPPL-2703 (1990), to be published J. Nucl. Mat. (1990).

[32] E. Fredrickson, private communication (1990).

[33] C.Z. Cheng, K.T. Tsang, Nucl. Fus. **21** 6 (1981) 643-650.

[34] V.M. Gribkov, D.Kh. Morosov, O.P. Pogutse,Proceedings of the Twelfth International Conference on Plasma Physics and Controlled Nuclear Fusion Research, (Nice, France, October 1988) (IAEA, Vienna, Austria) Paper IAEA-CN-38/U-1-2.

[35] T. S. Hahm, W. M. Tang, manuscript in preparation.

[36] T. S. Hahm, S. C. Cowley, J. C. Cummings, G. W. Hammett, R. M. Kulsrud, F. W. Perkins, *et al.* "Nonlinear Kinetic Analysis of Fluctuations and Turbulent Transport due to Tokamak Microinstabilities", IAEA. Washington, U.S. (1990).

Table 1: Summary of Experiments Simulated with PCDW

	ν^* <0.15	ν^* >0.15	η_i <1.5	η_i >1.5
•TFTR				
deuterium ohmic[3]		X		X
deuterium pellets [3,5]		X	X	
ohmic phase of supershot[3]	X			X
L-mode[6]		X		X
supershots[6,8]	X		X	
helium low density	X			X
helium high density		X		X
•T-10				
ohmic		X		X
ECH	X			X
•TEXT				
hydrogen low density[4]	X			X
hydrogen high density[4]		X		X
pellet[4]		X	X	
•Alcator-C				
ohmic[5]		X		X
pellet[5]		X	X	
•ASDEX				
ohmic[5]		X		X
pellet[5]		X	X	

Table 2: Plasma Parameters for Experiments Simulated

	Ohmic	L-mode	Supershot
Shot	31819	41326	30640
I_p(MA)	1.2	1.8	0.9
B_Z(T)	4.95	3.8	4.9
R(m)	2.36	2.58	2.46
a(m)	0.71	0.92	0.81
$\bar{n}_e(10^{19}/m^3)$	2.5	4.19	2.57
q_a^{cyl}	4.4	3.5	7.2
Z_{eff}	2.0	3.2	3.0
P_{inj}(MW)	0.	16.8	14.3

Table 3: Radially Integrated Heating and Losses at r = a/2 in MW

	Q^e_{cond}	Q^e_{conv}	Q^i_{cond}	Q^i_{conv}	Q_{Neut}	Q_{Rad}	Q_{heat}	Q_{ei}	ν^*_e	η_i
Ohmic										
PCDW	0.49	0.0022	0.14	0.0020	1.3×10^{-3}	0.11	0.75	0.15	0.2	2.4
MMM	0.12	–	0.32	–	0.012	0.074	0.51	0.32	–	–
MMCD	0.18	–	0.24	–	2×10^{-3}	0.083	0.50	0.23	–	–
L-mode										
PCDW	3.3	0.20	2.6	0.28	0.14	0.27	7.3	-1.6	0.11	4.5
MMM	2.2	–	3.9	–	0.13	0.27	7.2	-0.11	–	–
MMCD	1.7	–	5.3	–	-0.039	0.28	7.1	0.06	–	–
Supershot										
PCDW	2.5	0.74	2.1	2.6	0.62	0.64	10.	-1.6	0.05	0.8
MMM	3.2	–	3.8	–	0.21	0.69	8.2	-1.0	–	–
MMCD	2.7	–	5.2	–	0.18	0.92	9.3	-0.91	–	–

Table 4: Comparison of Measured and Simulated Plasma Performance for TFTR

	T_{eo} (keV)	T_{io} (keV)	τ_e^{th} (sec)	P_{OH} MW)	V_{Loop} (V)	β_T (%)	β_p
Ohmic							
experiment	2.9	2.2	0.252	0.76	0.63	0.069	0.12
PCDW	2.8	2.1	0.226	1.04	0.89	0.068	0.15
MMM	3.6	1.7	0.384	0.67	0.58	0.077	0.17
MMCD	2.9	1.8	0.365	0.79	0.67	0.084	0.18
L-mode							
experiment	4.5	3.7	0.064	0.68	0.38	0.40	0.37
PCDW	4.0	6.1	0.095	0.52	0.28	0.57	0.53
MMM	5.3	5.3	0.106	0.34	0.20	0.66	0.62
MMCD	4.4	4.6	0.122	0.30	0.05	0.71	0.67
Supershot							
experiment	7.9	23.	0.097	0.19	-0.21	0.55	1.8
PCDW	6.3	20.	0.088	0.14	-0.48	0.47	2.3
MMM	4.0	18.	0.059	0.47	-0.31	0.42	2.0
MMCD	4.5	10.	0.079	0.13	-0.39	0.49	2.4

Figures

Fig. 1 Simulated density for ohmic case using empirical density transport model (solid curve), MMM (dotted curve) and MMCD (dashed curve) compared to experiment.

Fig. 2 Simulated density for L-mode case using empirical density transport model (solid curve), MMM (dotted curve) and MMCD (dashed curve) compared to experiment.

Fig. 3 Simulated density for supershot case using empirical density transport model (solid curve), MMM (dotted curve) and MMCD (dashed curve) compared to experiment.

Fig. 4 (a) Simulations of electron temperature with PCDW (solid curve) and MMCD (dashed curve), MMCD' (long dashed curve), compared to TFTR data for ohmic shot 31819.

(b) Simulations of ion temperature with PCDW (solid curve) and MMCD (dashed curve), MMCD' (long dashed curve), compared to TFTR data for ohmic shot 31819.

(c) Simulation of electron temperature with PCDW (solid curve) and MMCD (dashed curve), MMCD' (long dashed curve), compared to

TFTR data for L-mode shot 41326.

(d) Simulation of ion temperature with PCDW (solid curve) and *MMCD (dashed curve), MMCD' (long dashed curve)*, compared to TFTR data for L-mode shot 41326.

(e) Simulation of electron temperature with PCDW (solid curve) and MMCD (dashed curve), MMCD' with $\eta_i^c = 10.$, (long dashed curve), compared to TFTR data for supershot 30640.

(f) Simulation of ion temperature with PCDW (solid curve) and MMCD (dashed curve), MMCD' with $\eta_i^c = 10.$, (iong dashed curve), compared to TFTR data for supershot 30640.

Fig. 5 (a) PCDW simulation of central electron and ion temperature evolution for TFTR supershot 30640.

(b) MMM simulation of central electron and ion temperature evolution for TFTR supershot 30640.

(c) MMCD simulation of central electron and ion temperature evolution for TFTR supershot 30640.

Fig. 6 (a) PCDW prediction of χ_e and χ_i for TFTR ohmic case.

(b) PCDW prediction of χ_e and χ_i for TFTR L-mode case.

(c) PCDW prediction of χ_e and χ_i for TFTR supershot case.

Fig. 7 MMCD prediction of multiple mode components of

(a) χ_e for TFTR ohmic shot 31819,

(b) χ_i for TFTR ohmic shot 31819.

(c) χ_e for TFTR L-mode shot 41326,

(d) χ_i for TFTR L-mode shot 41326,

(e) χ_e for TFTR supershot 30640,

(f) χ_i for TFTR supershot 30640. Here circles designate total diffusivity while 'triangles' designate TEM losses, 'crosses' designate η_i losses, and 'squares' designate resistive ballooning derived losses.

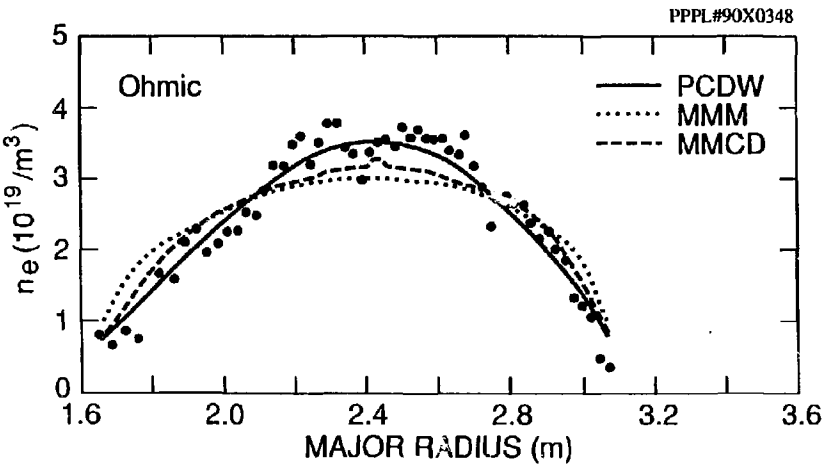
PPPL#90X0348
Ohmic
PCDW
MMM
MMCD
ne(10^19/m^3)
MAJOR RADIUS (m)
0
1
2
3
4
5
1.6
2.0
2.4
2.8
3.2
3.6

FIG. 1

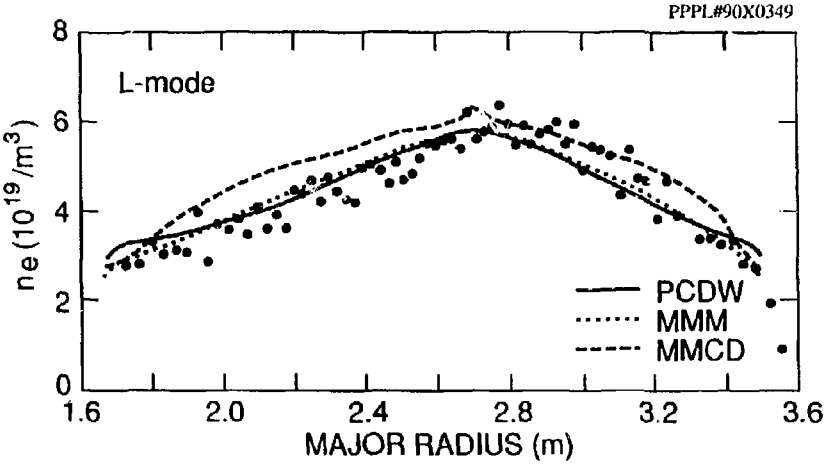
PPPL#90X0349
L-mode
ne(10^19/m^3)
8
6
4
2
0
1.6
2.0
2.4
2.8
3.2
3.6
MAJOR RADIUS (m)
PCDW
MMM
MMCD

FIG. 2

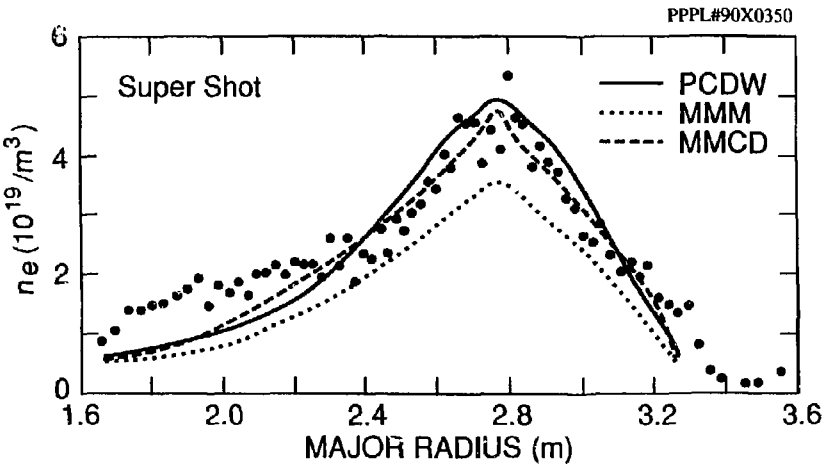
PPPL#90X0350
Super Shot
PCDW
MMM
MMCD
ne (10^19/m^3)
MAJOR RADIUS (m)
0
2
4
6
1.6
2.0
2.4
2.8
3.2
3.6

FIG. 3

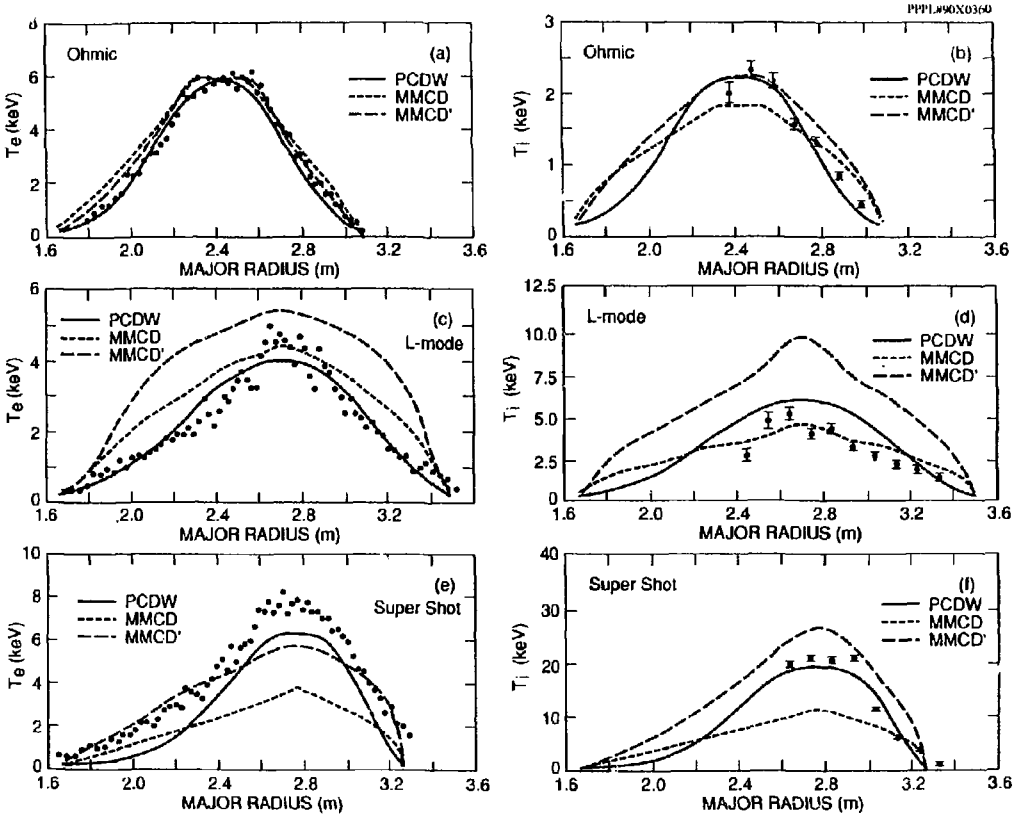
PPPL-90X0360
Ohmic
(a)
PCDW
MMCD
MMCD'
T_e (keV)
MAJOR RADIUS (m)
Ohmic
(b)
PCDW
MMCD
MMCD'
T_i (keV)
MAJOR RADIUS (m)
PCDW
MMCD
MMCD'
(c)
L-mode
T_e (keV)
MAJOR RADIUS (m)
L-mode
(d)
PCDW
MMCD
MMCD'
T_i (keV)
MAJOR RADIUS (m)
PCDW
MMCD
MMCD'
(e)
Super Shot
T_e (keV)
MAJOR RADIUS (m)
Super Shot
(f)
PCDW
MMCD
MMCD'
T_i (keV)
MAJOR RADIUS (m)

FIG. 4

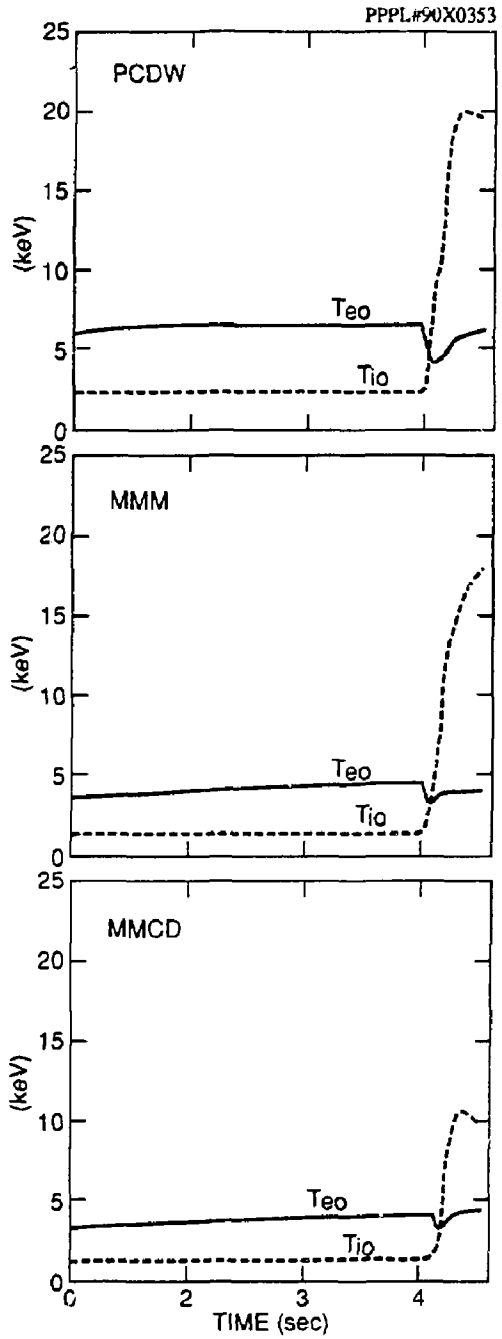
PPPL#90X0353
PCDW
MMM
MMCD
Teo
Tio
(keV)
TIME (sec)
0
5
10
15
20
25
2
3
4

FIG. 5

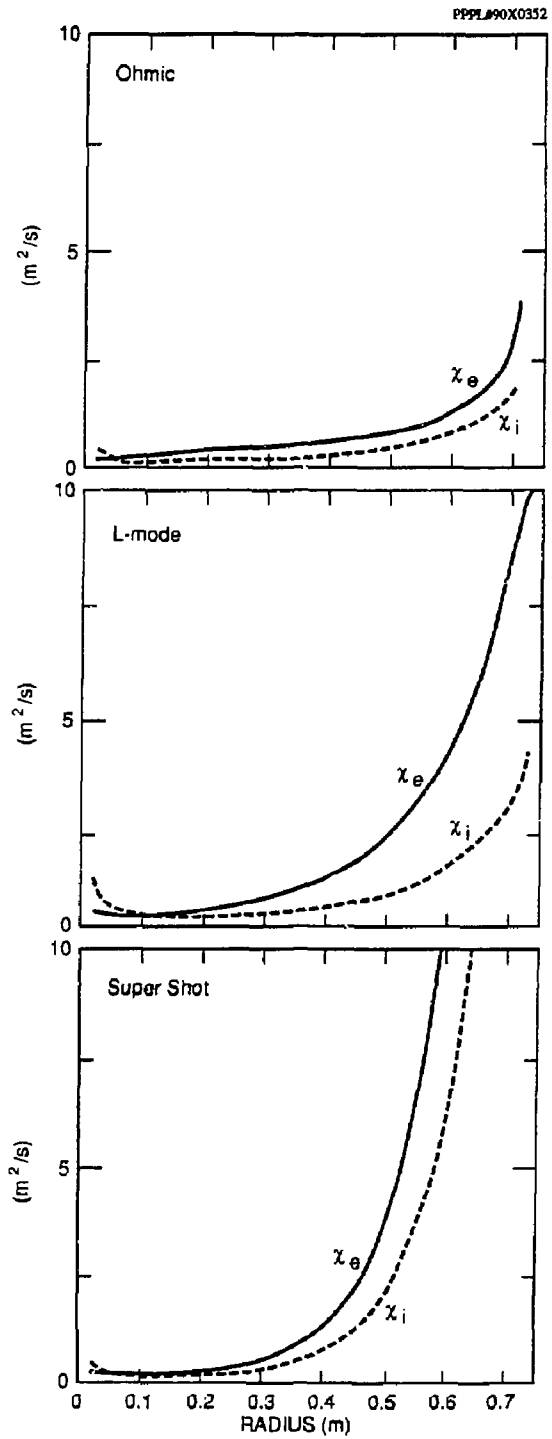
PPPL#90X0352
Ohmic
L-mode
Super Shot
(m²/s)
10
5
0
χe
χi
0
0.1
0.2
0.3
0.4
0.5
0.6
0.7
RADIUS (m)

FIG. 6

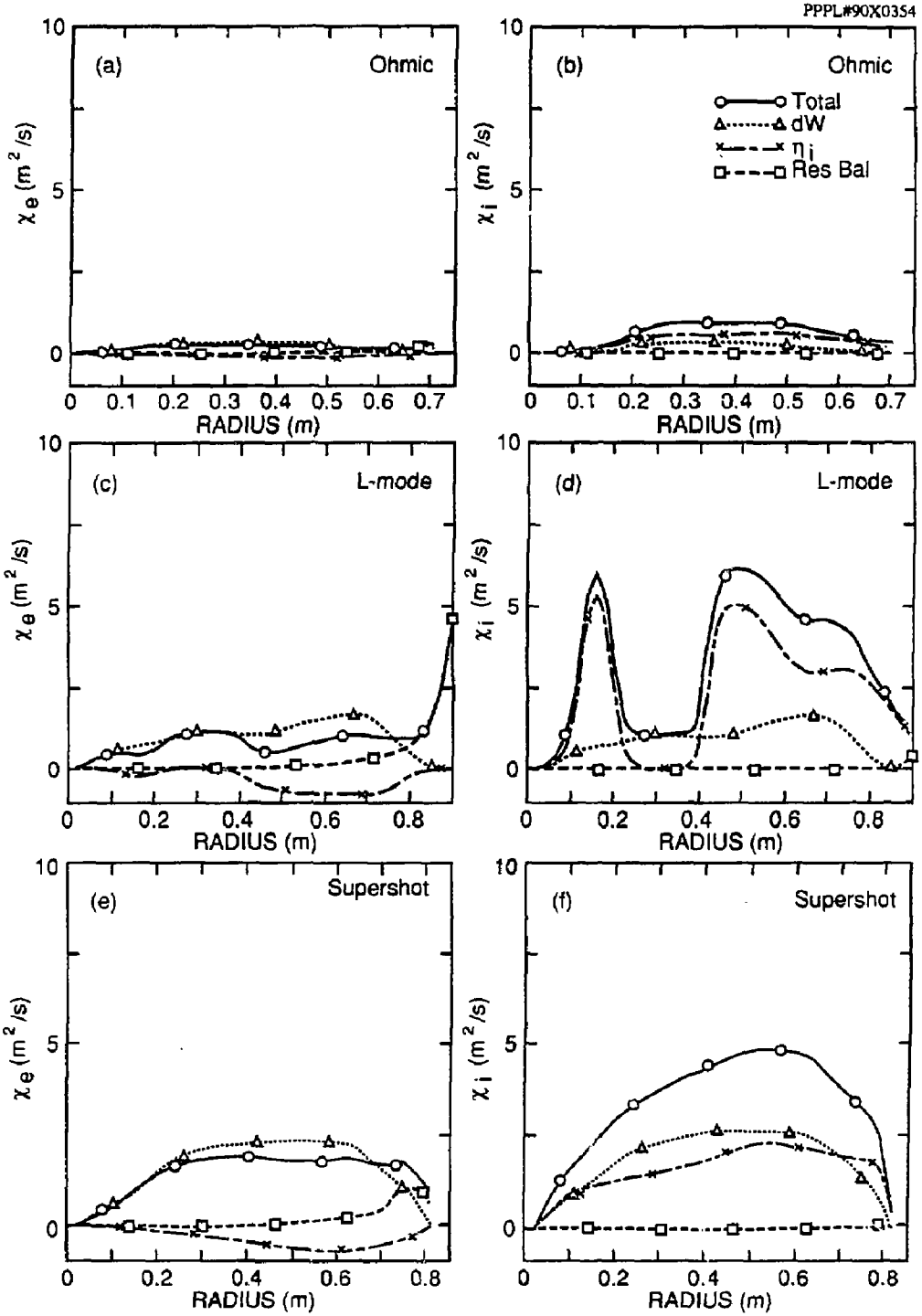
(a)
Ohmic
χ_e (m^2/s)
RADIUS (m)
(b)
Ohmic
Total
dW
η_i
Res Bal
χ_i (m^2/s)
RADIUS (m)
(c)
L-mode
χ_e (m^2/s)
RADIUS (m)
(d)
L-mode
χ_i (m^2/s)
RADIUS (m)
(e)
Supershot
χ_e (m^2/s)
RADIUS (m)
(f)
Supershot
χ_i (m^2/s)
RADIUS (m)

FIG. 7